Acta Crystallographica Section D
Biological Crystallography
ISSN 0907-4449

Structural analysis of an MK2–inhibitor complex: insight into the regulation of the secondary structure of the Gly-rich loop by TEI-I01800

Aiko Fujino, Kei Fukushima, Naoko Namiki, Tomomi Kosugi and Midori Takimoto-Kamimura*

Teijin Institute for Biomedical Research, Japan

Correspondence e-mail: m.kamimura@teijin.co.jp

Received 6 July 2009
Accepted 4 November 2009

PDB Reference: MK2–TEI-I01800 complex, 3a2c.

Mitogen-activated protein kinase-activated protein kinase 2 (MAPKAP-K2 or MK2) is a Ser/Thr kinase from the p38 mitogen-activated protein kinase signalling pathway and plays an important role in inflammatory diseases. The crystal structure of the complex of human MK2 (residues 41–364) with the potent MK2 inhibitor TEI-I01800 (pK_i = 6.9) was determined at 2.9 Å resolution. The MK2 structure in the MK2–TEI-I01800 complex is composed of two domains, as observed for other Ser/Thr kinases; however, the Gly-rich loop in the N-terminal domain forms an α-helix structure and not a β-sheet. TEI-I01800 binds to the ATP-binding site as well as near the substrate-binding site of MK2. Both TEI-I01800 molecules have a nonplanar conformation that differs from those of other MK2 inhibitors deposited in the Protein Data Bank. The MK2–TEI-I01800 complex structure is the first active MK2 with an α-helical Gly-rich loop and TEI-I01800 regulates the secondary structure of the Gly-rich loop.

1. Introduction

Mitogen-activated protein kinase-activated protein kinase 2 (MAPKAP-K2 or MK2) is a Ser/Thr kinase from the p38 mitogen-activated protein (MAP) kinase signalling pathway. The p38 MAP kinase pathway plays an important role in the production of TNF-α and various cytokines (Beyaert *et al.*, 1996). TNF-α causes many types of inflammatory diseases such as arthrorheumatism, for which anti-TNF-α antibodies such as infliximab are the most effective medications. TNF-α is thus a promising target for anti-inflammatory therapy.

The p38 MAP kinase inhibitors SB203580 and BIRB-796 inhibit LPS-induced cytokine synthesis (Lee *et al.*, 1994; Pargellis *et al.*, 2002; Gruenbaum *et al.*, 2009) and also prevent phosphorylation and activation of MK2 (Cuenda *et al.*, 1995). As MK2-knockout mice showed a reduction in TNF-α, interferon-γ, IL-1β and IL-6, MK2 was shown to be essential for LPS-induced TNF-α biosynthesis (Kotlyarov *et al.*, 1999). MK2 plays an important role in TNF-α biosynthesis and is a novel target for the development of new small-molecule drugs for oral administration. Several pharmaceutical companies have reported new small-molecule inhibitors of MK2 (Hillig *et al.*, 2007; Anderson *et al.*, 2007, 2009; Wu *et al.*, 2007; Goldberg *et al.*, 2008; Xiong *et al.*, 2008; Argiriadi *et al.*, 2009).

The apo structure of MK2 was first determined in 2002 (Meng *et al.*, 2002) and the structures of the MK2–AMPPNP (Kurumbail *et al.*, 2003), MK2–ADP and MK2–staurosporine complexes were determined in 2003 (Underwood *et al.*, 2003).

Several structures of MK2 complexed with small-molecule inhibitors have been reported and their structure–activity relationships have been discussed (Hillig *et al.*, 2007; Anderson *et al.*, 2007, 2009; Wu *et al.*, 2007). Both the apo MK2 and the MK2–AMPPNP structures represent inactive conformations (with the Lys93–Glu104 salt bridge disrupted). Apo MK2 has an α-helical Gly-rich loop (α-form), while MK2–AMPPNP has a β-sheet Gly-rich loop (β-form). In contrast, the structures of the complexes of active MK2 (amino-acid residues 41–364 or 45–371) with ADP, staurosporine and various small-molecule inhibitors all have the β-form. Although these constructs contain part of the autoinhibitory domain sequence that associates with the substrate-binding region, these sequences are disordered. In particular, the 41–364 construct of MK2 has been reported to be constitutively active without phosphorylation by p38 MAP kinase (Underwood *et al.*, 2003). Therefore, the α-form of apo MK2 was considered to be an artificial structure that was produced as an effect of mercury modification (Underwood *et al.*, 2003). However, the secondary structure of the Gly-rich loop of active MK2 has not been focused on in previous reports on MK2 and other kinases.

In the present study, we determined the structure of human MK2 complexed with the potent inhibitor TEI-I01800 at 2.9 Å resolution. The results showed that the Gly-rich loop of the MK2–TEI-I01800 complex formed an α-helix and differs from other reported MK2–small-molecule inhibitor complexes. Here, we report the crystal structure of the MK2–TEI-I01800 complex and suggest that the structural features of TEI-I01800 are important in regulating the secondary structure of the Gly-rich loop.

2. Materials and methods

2.1. Cloning, expression and purification

The expression plasmids were constructed as described by Underwood *et al.* (2003). The human MK2 kinase domain (residues 41–364) was amplified by PCR using oligonucleotide primers, inserted between the *Nde*I and *Xho*I sites of pET-22b(+) (Novagen) and then transformed into *Escherichia coli* strain BL21 (DE3) (Novagen). These cultures were grown to an OD_{600} of 0.7 and expression was carried out in LB medium containing 100 µg ml^{-1} ampicillin with 1 m*M* isopropyl β-D-1-thiogalactoside (IPTG) at 298 K for about 3 h. The cell pellets from 500 ml culture were suspended in 50 ml buffer *A* (20 m*M* HEPES pH 7.5, 10 m*M* NaCl and 5 m*M* DTT) and sonicated on ice. The supernatant was applied onto a Q Sepharose HP column (GE Healthcare) and the flowthrough sample was collected. The solution containing MK2 protein was applied onto a Resource S column (GE Healthcare) and eluted using a linear gradient to buffer *B* (20 m*M* HEPES pH 7.5, 500 m*M* NaCl and 5 m*M* DTT). The fraction containing MK2 was applied onto a Superdex 75 gel-filtration column (GE Healthcare) equilibrated with buffer *C* (20 m*M* HEPES pH 7.5, 200 m*M* NaCl and 5 m*M* DTT) and the fractions containing a single peak were collected. The purified human MK2 was concentrated to 5–20 mg ml^{-1} in buffer *D* (20 m*M* HEPES pH 7.5, 5 m*M* $MgCl_2$, 200 m*M* NaCl and 10 m*M* DTT) before crystallization.

Table 1
Data-collection and refinement statistics.

Values in parentheses are for the highest resolution shell.

Data collection	
Beamline	SPring-8 BL32B2
Wavelength (Å)	1.000
Resolution (Å)	50.0–2.90 (3.00–2.90)
Mosaicity (°)	0.32
No. of unique reflections	121109
R_{merge} (%)	9.1 (44.7)
Completeness (%)	99.8 (99.0)
Multiplicity	5.7 (4.5)
Average $I/\sigma(I)$	24.7 (3.3)
Space group	$P2_12_12_1$
Unit-cell parameters (Å)	
a	139.15
b	180.95
c	216.09
Refinement	
Resolution (Å)	20-2.9
R factor (%)	28.8
R_{free} (%)	33.5
No. of reflections (work/test)	114397/6068
R.m.s.d. from ideal values	
Bond lengths (Å)	0.012
Bond angles (°)	1.28
Ramachandran statistics	
Most favoured regions (%)	87.7
Additional allowed regions (%)	12.0
Generously allowed regions (%)	0.3
Disallowed regions (%)	0.0

2.2. Crystallization and data collection

The kinase domain of MK2 is known to be a difficult crystallization target and all MK2 crystals described to date diffracted to only low or medium resolution (Meng *et al.*, 2002; Kurumbail *et al.*, 2003; Underwood *et al.*, 2003; Hillig *et al.*, 2007; Anderson *et al.*, 2007, 2009; Wu *et al.*, 2007; Goldberg *et al.*, 2008; Xiong *et al.*, 2008; Argiriadi *et al.*, 2009). The first MK2–TEI-I01800 crystal was obtained under similar conditions to those reported previously (Underwood *et al.*, 2003). However, it diffracted to low resolution and was predicted to belong to space group $P2_12_12_1$ with 12 molecules in the asymmetric unit. Therefore, cocrystallizations were performed using commercially available screening kits consisting of more than 1000 conditions and soaking using both apo MK2 and MK2–ADP. Several crystals were obtained in various conditions, but they all diffracted to low resolution and belonged to the same space group with similar unit-cell parameters. Optimized MK2–TEI-I01800 crystals were obtained by the cocrystallization method and were grown in 0.1 *M* HEPES pH 7.5, 1.6–2.0 *M* ammonium sulfate and 5% ethanol. All crystallizations were performed at 293 K using the sitting-drop vapour-diffusion method. After soaking in cryoprotectant buffer containing 30% sucrose, a data set was collected at 100 K on the SPring-8 BL32B2 beamline using an R-AXIS IV image-plate detector. The MK2–TEI-I01800 crystals diffracted to less than 2.9 Å resolution and belonged to space group

$P2_12_12_1$, with unit-cell parameters a = 139.15, b = 180.95, c = 216.09 Å and 12 molecules in the asymmetric unit (Matthews coefficient V_M = 3.03 Å^3 Da^{-1}, solvent content V_{solv} = 59.3%). The reflection data were processed using the *HKL*-2000 software package (Otwinowski & Minor, 1997). The data-processing and refinement statistics are shown in Table 1.

2.3. Structure determination and refinement

Structure determination was performed by molecular replacement using the MK2 protein from the MK2–ADP complex (PDB code 1ny3; Underwood *et al.*, 2003) as a search model. Several programs were used, but only *MOLREP* (Vagin & Teplyakov, 1997) found six of the 12 molecules in the asymmetric unit, with corr(I) = 42.0 and R = 54.7%. However, an $F_o - F_c$ electron-density map calculated with six molecules showed clear positive blobs that were recognizable as MK2 molecules (R = 43.1%, R_{free} = 49.8%). Consequently, after density modification by NCS averaging (Bricogne, 1974; Schuller, 1996) using *DM* (Cowtan, 1994) in the *CCP*4 suite (Collaborative Computational Project, Number 4, 1994), a further six molecules were assigned manually in the density maps using *QUANTA* (Accelrys Inc.; http://accelrys.co.jp/). In this process, every time a molecule was found rigid-body and restrained refinement were performed using *REFMAC* (Murshudov *et al.*, 1997) to check the R factor and a new electron-density map was calculated. After the determination of 12 MK2 molecules, the R and R_{free} factors fell to 27.9% and 37.6%, respectively. At this stage, the $F_o - F_c$ map clearly showed a positive blob-shaped TEI-I01800 molecule at the ATP-binding site in each molecule; 12 TEI-I01800 molecules were assigned by *QUANTA*/*X-LIGAND* and the R and R_{free} factors fell to 21.5% and 29.4%, respectively. Moreover, positive peaks appeared near the substrate-binding pockets in the $F_o - F_c$ map and an additional 12 TEI-I01800 molecules were assigned as previously. The structure of the MK2–TEI-I01800 complex was then refined to R and R_{free} factors of 20.9% and 29.2%, respectively. We found that both $2F_o - F_c$ and $F_o - F_c$ maps showed a different structure around the Gly-rich loop in the current protein model compared with the search model. The Gly-rich loops in 12 molecules were rebuilt based on an OMIT map and structure refinement was continued to R and R_{free} factors of 20.2% and 28.7%, respectively. However, the r.m.s.d.s of the bond lengths and torsion angles from ideal values were very large and were not improved by *REFMAC*. Consequently, after conversion to *CNX* (Accelrys Inc.; http://accelrys.co.jp/) format with the

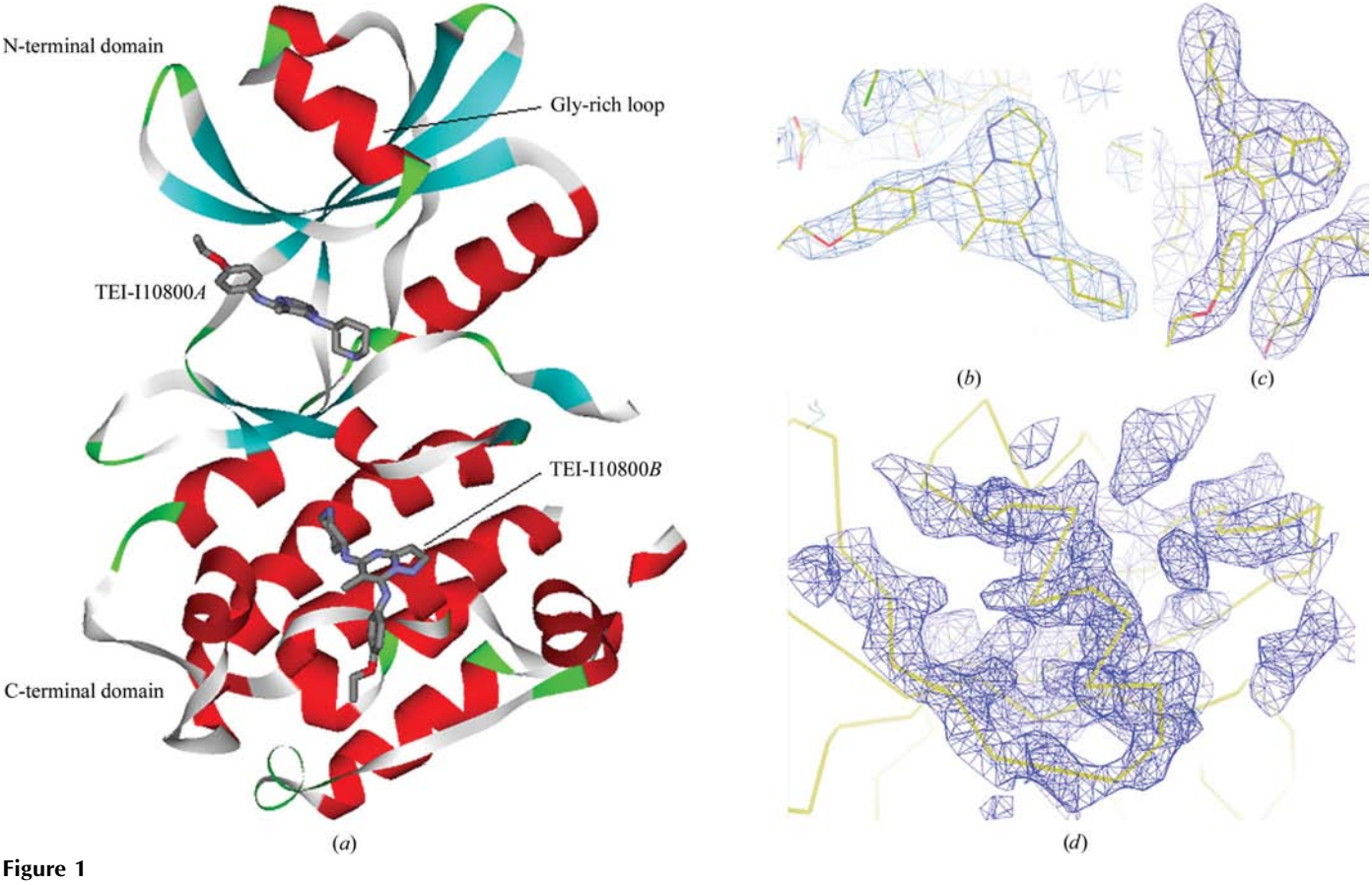

Figure 1
Structure of molecule A of MK2–TEI-I01800 and $2F_o - F_c$ maps (contoured at 1.0σ). (*a*) The overall kinase fold and the binding of TEI-I01800*A* in the ATP-binding site and of TEI-I01800*B* in the substrate-binding site of MK2. The overall fold of MK2 is shown in ribbon representation (α-helices are shown in red, β-sheets in blue and β-turns in green). Two inhibitors are shown in stick representation. TEI-I01800*A* (*b*), TEI-I01800*B* (*c*) and the Gly-rich loop (*d*) could be placed in the density maps despite the low resolution.

same R_{free} flags, torsion-angle refinement was carried out automatically using the *LAFIRE* program (Yao *et al.*, 2006; Zhou *et al.*, 2006) running with the refinement program *CNX* with NCS restraints. The final R and R_{free} factors were 28.8% and 33.5%, which were larger than the previous values; however, the r.m.s.d. values and Ramachandran statistics were dramatically improved. The coordinates and structure factors have been deposited in the PDB with code 3a2c. Figures were produced using *DS Visualizer* (Accelrys; http://accelrys.co.jp/).

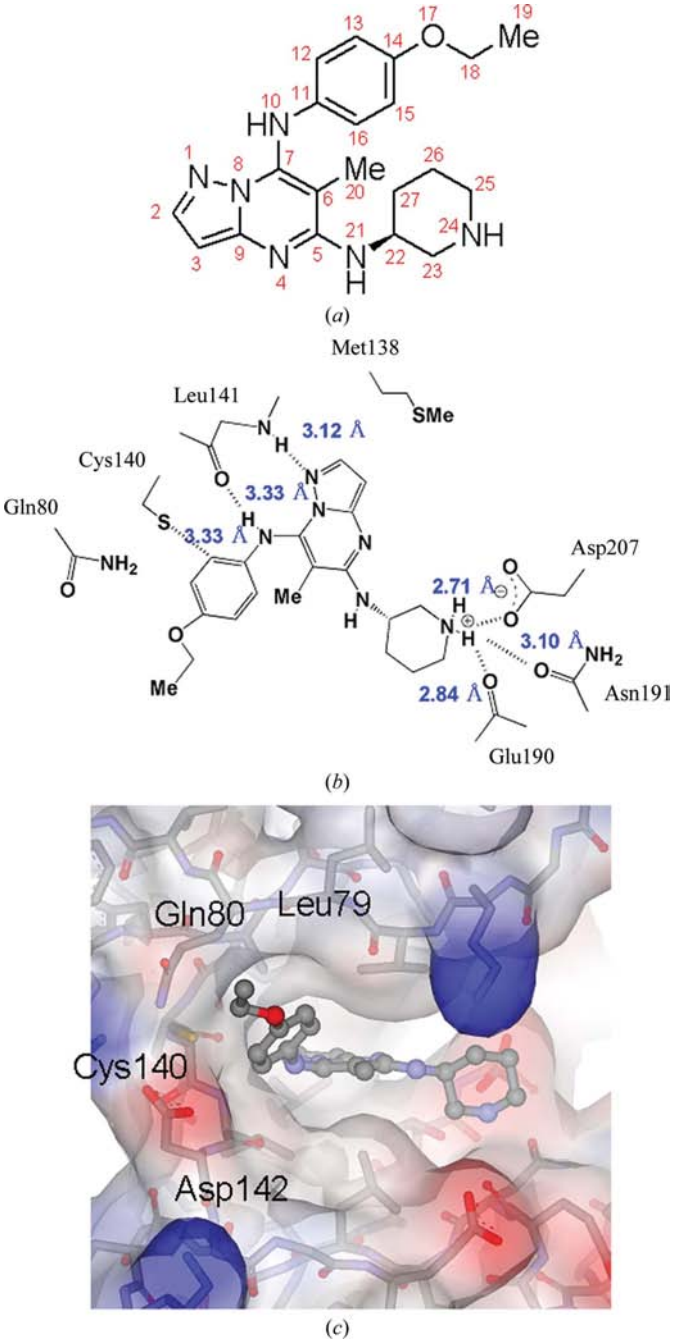

Figure 2
Interactions of TEI-I01800*A* in the ATP-binding site of MK2. (*a*) Schematic molecular structure of TEI-I01800. Atom numbers were assigned sequentially. The bonds C7—N10 and N10—C11 between the pyrazolo[1,5-*a*]pyrimidine-scaffold part and the *p*-ethoxyphenyl group at the 7-position are freely rotatable. (*b*) Binding interaction of TEI-I01800*A* and MK2. (*c*) Solvent-accessible surface view of the new binding pocket for TEI-I01800*A* (blue shows the electrostatic positive charge and red shows the negative charge as calculated by *DS Visualizer*).

3. Results and discussion

3.1. Structure of the MK2–TEI-I01800 complex

3.1.1. Overall structure. There are 12 MK2–TEI-I01800 complexes in the asymmetric unit of the $P2_12_12_1$ crystal constituting four trimers (described as chains *ABC*, *DEF*, *GHI* and *JKL*) that form a ring. In a trimer, each molecule interacts with neighbouring molecules in the substrate-binding pocket. This crystal-packing and oligomerization state is the same as in the complex of MK2 with the pyrrolopyrimidine analogue compound-1 (Hillig *et al.*, 2007). The r.m.s.d.s on C^{α} atoms between the monomers of MK2–TEI-I01800 are almost the same and are less than 1 Å. Molecule *A*, which has the lowest average *B* factor, was selected as the monomer structure that is discussed below.

The monomer structure of MK2–TEI-I01800 contains two domains (N-terminal and C-terminal domains) as in other kinases and is shown in Fig. 1(*a*). In the MK2–TEI-I01800 complex one MK2 molecule is bound by two TEI-I01800

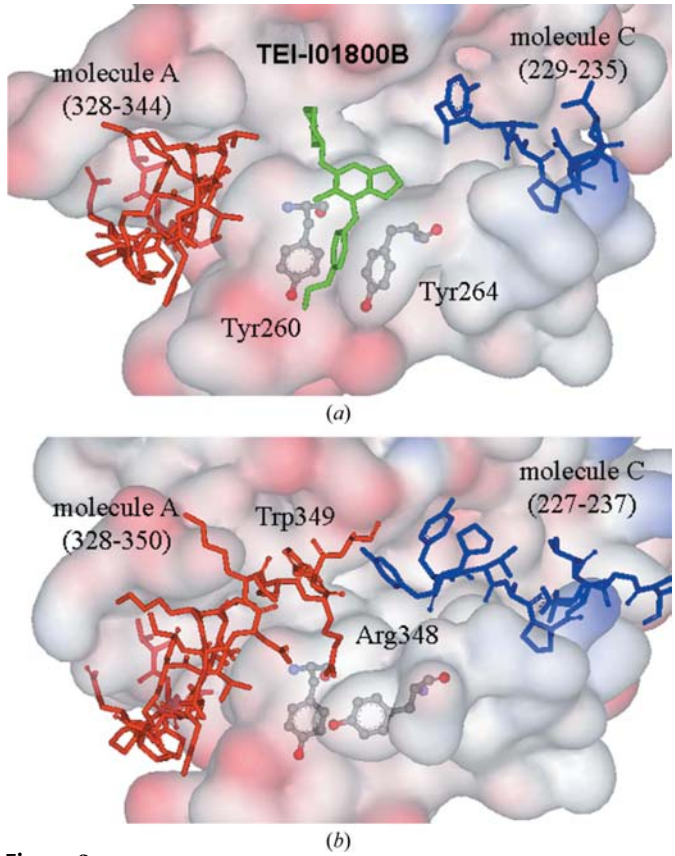

Figure 3
Substrate-binding pockets of (*a*) MK2–TEI-I01800*B* and (*b*) MK2–compound-1 (PDB code 2jbp; Hillig *et al.*, 2007) viewed from the same angle. TEI-I01800*B* binds between part of the auto-inhibitory domain and residues from the neighbouring molecule. The interaction sites of the 5- and 6-positions of TEI-I01800*B* are occupied by Arg348 and Trp349 in the case of MK2–compound-1.

molecules. The first TEI-I01800 molecule (TEI-I01800*A*) is bound to the ATP-binding site between the N-terminal and C-terminal domains. The second TEI-I01800 molecule (TEI-I01800*B*) interacts with MK2 near the substrate-binding site in the C-terminal domain. Figs. 1(*b*) and 1(*c*) show the electron-density maps for TEI-I01800*A* and TEI-I-1800*B*, respectively. Two inhibitors could be placed in the $F_o - F_c$ map despite the low resolution. The most notable feature of this complex is the Gly-rich loop in the N-terminal domain. In the MK2–TEI-I01800 complex all 12 molecules contain an α-helical Gly-rich loop. The initial density map calculated using the MK2–ADP complex (Underwood *et al.*, 2003) clearly showed a negative $F_o - F_c$ map around the β-sheet Gly-rich loop. Therefore, the corresponding residues were placed in the positive blobs by manual C^α tracing. After rebuilding the Gly-rich loop, the secondary structure was similar to that of the α-helical Gly-rich loop of the apo MK2 structure. The electron-density map for the α-helical Gly-rich loop of molecule *A* is shown in Fig. 1(*d*).

With the exception of the apo MK2 structure (Meng *et al.*, 2002), the Gly-rich loops of all other MK2s have the β-form. In these structures, each Gly-rich loop covers the ATP-binding site to stabilize ADP, staurosporine and other inhibitors. However, the ATP-binding site in the MK2–TEI-I01800 complex opens and is larger than that of MK2s with the β-sheet Gly-rich loop.

3.1.2. Binding mode and structure of TEI-I01800. The molecular structure and atomic numbering of TEI-I01800 are shown in Fig. 2(*a*). It has a pyrazolo[1,5-*a*]pyrimidine scaffold with a (3*S*)-piperidylamino group at the 5-position, a methyl group at the 6-position and a *p*-ethoxyphenylamino group at the 7-position. Its inhibitory activity for MK2 is $pK_i = 6.90$. The binding mode of TEI-I01800*A* is shown in Fig. 2(*b*). TEI-I01800*A* interacts with the backbone amide of Leu141 through two hydrogen bonds: TEI-I01800*A* N1···Leu141 N (3.12 Å) and TEI-I01800*A* N10···Leu141 O (3.33 Å). The N24 atom of TEI-I01800*A* must be ionized by hydrogen bonding to the carboxyl group of Asp207 (2.71 Å). This atom also makes two additional hydrogen bonds to the backbone carbonyl O atom of Glu190 (2.84 Å) and OD1 of Asn191 (3.10 Å). The (3*S*)-piperidylamino group is important for the MK2 inhibitory activity of TEI-I01800. Another notable interaction is the van der Waals interaction between C12/C16 of the *p*-ethoxyphenyl group at the 7-position and the S atom of Cys140. This *p*-ethoxyphenyl group is also important for the MK2 inhibitory activity; the inhibitory activity decreased when the *p*-ethoxyphenyl group was removed (unpublished data). As a result of the structural change from β-form to α-form MK2, a new pocket consisting of Leu79, Gln80, Cys140 and Asp142 is exposed and interacts with the *p*-ethoxyphenyl group at the 7-position (shown in Fig. 2*c*). In the β-sheet Gly-rich loop structure, part of the β-sheet covers and hides this pocket. However, in the α-form MK2 structure residues ^{65}VTSQVLGLGINGKVLQ^{80} are moved a maximum distance of 13.7 Å (for the Gly71 C^α atom) compared with the β-form and the new pocket is available for TEI-I01800*A* binding. TEI-I01800*A* is twisted around two freely rotatable bonds (C7—N10 and N10—C11) and interacts with this pocket (Figs. 2*b* and 2*c*). The methyl group at the 6-position is also important to induce the twisted conformation of the *p*-ethoxyphenylamino group at the 7-position. When the methyl group at the 6-position was removed from TEI-I01800, the inhibitory activity and selectivity clearly decreased (unpublished data). MK2–TEI-I01800 is the first structure to be determined of an α-form MK2 complexed with a small-molecule inhibitor and shows that the molecular properties of TEI-I01800*A* cause a secondary-structural change of the Gly-rich loop from a β-sheet to an α-helix.

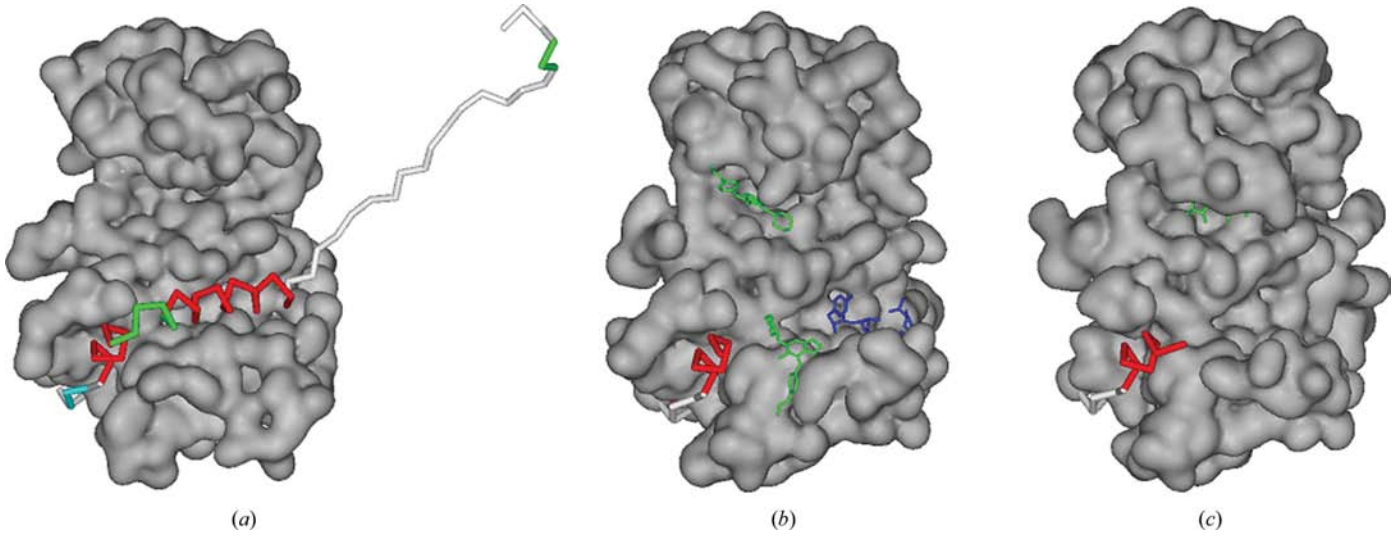

Figure 4
Surfaces of MK2. The C^α wire shows the auto-inhibitory domain (328–400); the inhibitors are shown in green and the residues from the neighbouring molecule that form a trimer are shown in blue. (*a*) Apo MK2 (PDB code 1kwp; Meng *et al.*, 2002). The substrate pocket is buried by the auto-inhibitory domain. The Gly-rich loop adopts an α-helical conformation and shows a wide-open ATP-binding pocket. (*b*) MK2–TEI-I01800. TEI-I01800*A* binds in the wide-open ATP-binding pocket exposed by the α-form Gly-rich loop. TEI-I01800*B* binds in the substrate-binding pocket. (*c*) MK2–ADP: an active β-form MK2. The ATP molecule binds in the narrow and closed ATP-binding site.

For the binding of TEI-I01800*B*, the *p*-ethoxyphenylamino group at the 7-position of the compound is positioned between the side chains of Tyr260 and Tyr264 (Fig. 3*a*). Tyr264 is stacked with the *p*-ethoxyphenyl group by a π–π interaction and there is no hydrogen-bonding interaction between MK2 and TEI-I01800*B*. The *p*-ethoxyphenyl group at the 7-position of TEI-I01800 might be crucial for the binding of TEI-I01800*B* to the substrate-binding pocket of MK2.

3.2. Structure comparison with apo MK2 and other MK2–inhibitor complexes

The first crystal structure of MK2 to be determined was the apo form (Meng *et al.*, 2002). It is an α-form MK2 in which the auto-inhibitory domain interacts with the substrate-binding pocket. Since its determination, the structures of MK2–AMPPNP, MK2–ADP, MK2–staurosporine and various MK2–small-molecule inhibitor complexes have been reported (Kurumbail *et al.*, 2003; Underwood *et al.*, 2003; Hillig *et al.*, 2007; Anderson *et al.*, 2007, 2009; Wu *et al.*, 2007). All of these complex structures show a β-form MK2 with a narrow and deep ATP-binding pocket.

In the MK2–TEI-I01800 complex crystal TEI-I01800*B* also binds to MK2 in the substrate-binding pocket. Fig. 3 shows a comparison of the substrate-binding pockets in MK2–TEI-I01800*B* and MK2–compound-1 (Hillig *et al.*, 2007). TEI-I01800*B* is sandwiched between part of the auto-inhibitory domain (molecule *A*, 328–344) and the neighbouring molecule (molecule *C*, 229–235) and the substrate-binding pocket is filled by TEI-I01800*B* and these residues (Fig. 3*a*). In MK2–compound-1, amino-acid residues 328–350 from molecule *A* and the active segment (amino-acid residues 227–237) from molecule *C* fill this active pocket as shown in Fig. 3(*b*) and therefore it has been proposed that it may represent an intermediate state during substrate phosphoryration (Hillig *et al.*, 2007). In the MK2–TEI-I01800 complex the density map for residues 345–350 was not visible. In the case of MK2–TEI-I01800 the auto-inhibitory domain may have been pushed out into the solvent area by the binding of TEI-I01800*B*. We also attempted to confirm the binding affinity for TEI-I01800*B* using BIACORE 3000 (GE Healthcare), but the result showed that at least one TEI-I01800 could bind to MK2. In addition, the substrate-competitive bioassay did not show binding of TEI-I01800 in the substrate-binding pocket. Therefore, the binding of the TEI-I01800*B* molecule is considered to be very weak and not suitable for drug discovery.

The Lys93–Glu104 salt bridge is essential in active kinases (Huse & Kuriyan, 2002). Apo MK2 is in an inactive kinase conformation because the Lys93–Glu104 salt bridge is disrupted and the substrate-binding site is blocked by the auto-inhibitory domain (Fig. 4*a*). Apo MK2 has an α-helical Gly-rich loop. In contrast, MK2–AMPPNP has a different inactive conformation (with Lys93–Glu104 salt-bridge disruption) that maintains the β-sheet Gly-rich loop (Kurumbail *et al.*, 2003). Other MK2–small-molecule complexes (MK2–ADP is shown in Fig. 4*c*) apart from MK2–AMPPNP all show active conformations with a Lys93–Glu104 salt bridge and a β-sheet Gly-rich loop. The β-sheet Gly-rich loop has been considered to be a characteristic feature of active MK2, but the MK2–TEI-I01800 complex is the first active MK2 structure to have a Lys93–Glu104 salt bridge and an α-helical Gly-rich loop (Fig. 4*b*).

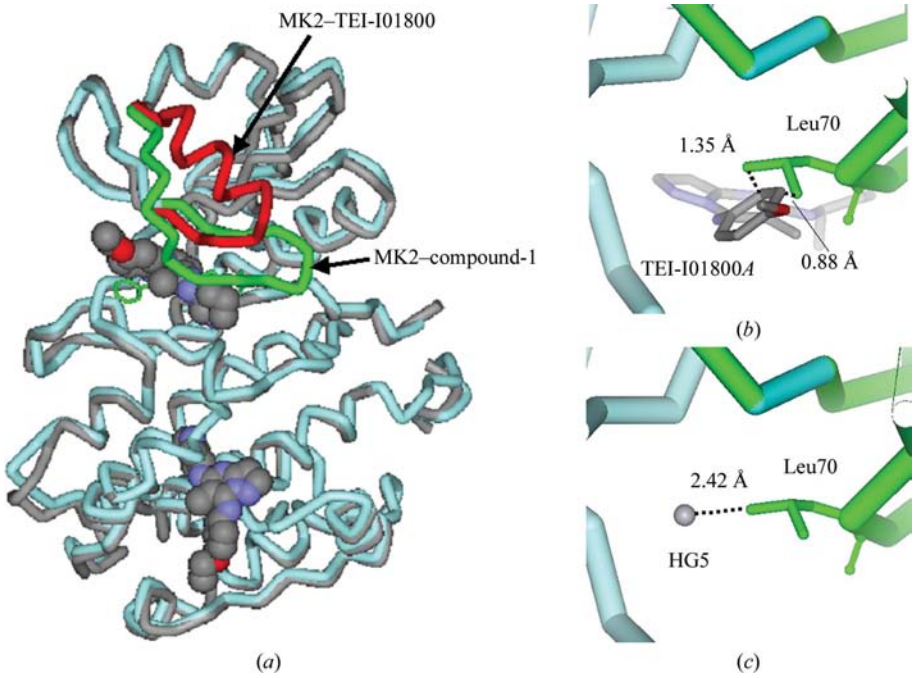

Figure 5
Superposition of MK2–TEI-I1800 and apo MK2 onto β-form MK2. (*a*) MK2–TEI-I01800 (grey) is superposed onto β-form MK2 (MK2–compound-1, blue). The r.m.s.d. on C^{α} atoms is 2.01 Å. The Gly-rich loop residues 65–80 of MK2–TEI-I01800 are shown in red and those of MK2–compound-1 are shown in green. (*b*) View of the conflict between TEI-I01800 and Leu70 CD1 of β-form MK2, (*c*) view of the conflict between HG5 and Leu70 CD1 of β-form MK2 on superposing apo MK2 onto MK2–compound-1. The r.m.s.d. on C^{α} atoms is 3.17 Å.

Consequently, we determined the features that cause the structural change of active MK2 from the β-form to the α-form. Fig. 5(*a*) shows a superimposed image of MK2–TEI-I01800 onto MK2–compound-1 (the r.m.s.d. on C^{α} atoms between MK2 in the MK2–TEI-I01800 complex and MK2 in the MK2–compound-1 structure is 2.01 Å). The most distinctive difference is in the structure of the Gly-rich loop. Fig. 5(*b*) shows that TEI-I01800*A* would be in conflict with the side chain of Leu70 of the Gly-rich loop if MK2 took the β-form (a distance of 1.35 Å between C12/C16 and Leu70 CD1 and an abnormally short distance of 0.83 Å between C13/C15 and Leu70 CD2). On the other hand, Fig. 5(*c*) shows a view of the conflict between Leu70 and Hg atom HG5 on superimposing apo MK2 onto MK2–compound-1 (the r.m.s.d. on

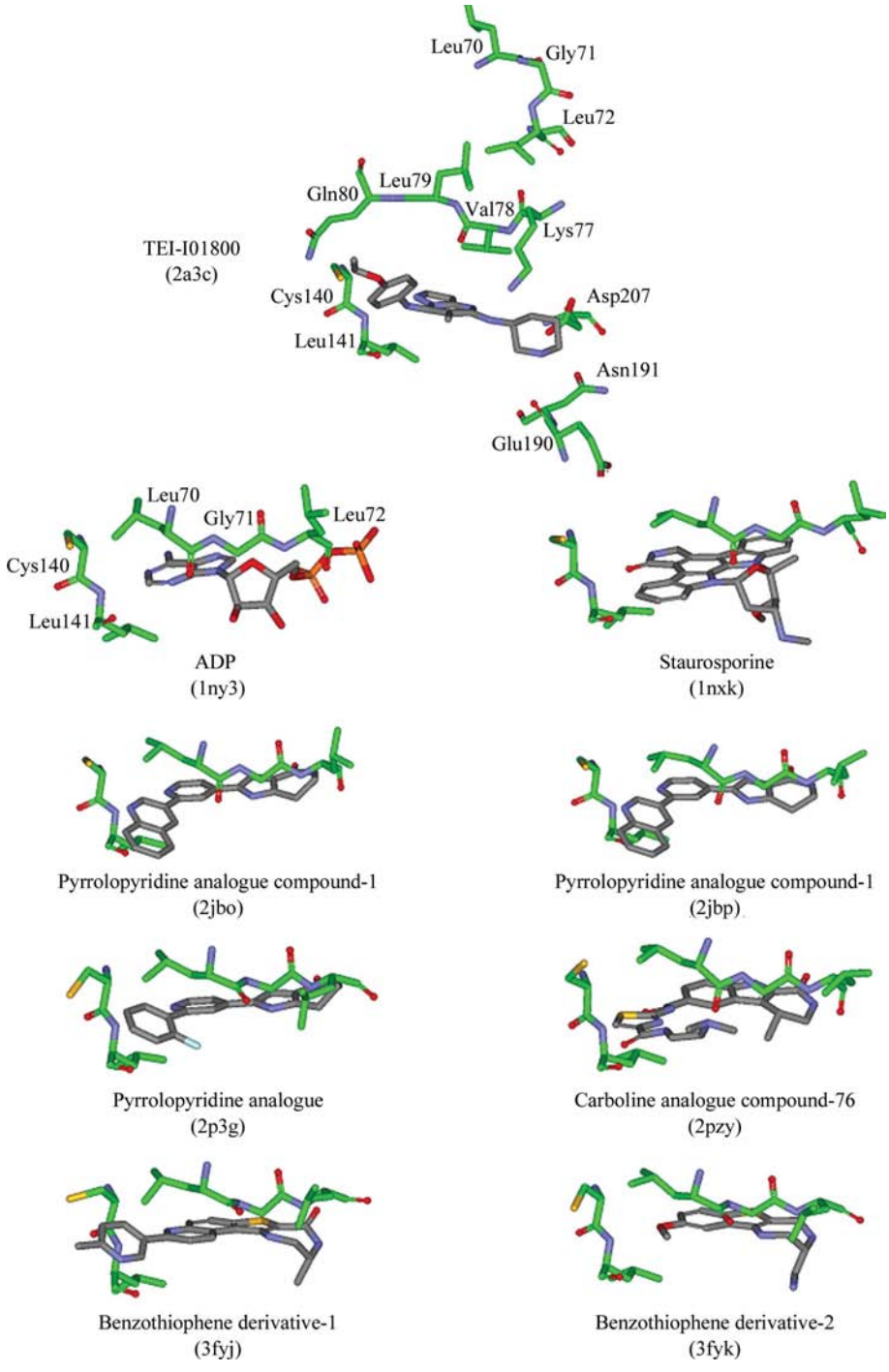

Figure 6
Three-dimensional structures of compounds bound to MK2. The compound names are shown under the structures and PDB codes are shown in parentheses. In MK2–TEI-I01800 (PDB code 2a3c), Leu70–Leu72 and Lys77–Gln80 of the α-helical Gly-rich loop and the residues that interact with TEI-I01800 are shown. In the other complexes, Leu70–Leu72 of the β-sheet Gly-rich loop, Cys140 and Leu141 are shown in green. The directions of these are matched. Only TEI-I01800 regulates the Gly-rich loop and interacts with Cys140 and Leu141.

C^{α} atoms between these structures is 3.17 Å). The Hg atom of apo MK2 also might conflict with the β-sheet Gly-rich loop (the distance between Hg atom HG5 and Leu70CD1 is 2.42 Å). In order to avoid those conflicts with Leu70, MK2–TEI-I01800 and apo MK2 adopt an α-helical Gly-rich loop. The TEI-I01800*A* molecule regulates the secondary structure of the Gly-rich loop of MK2.

3.3. TEI-I01800 regulates the secondary structure of the Gly-rich loop

TEI-I01800 has two freely rotatable bonds between the pyrazolo[1,5-*a*] pyrimidine scaffold part and the *p*-ethoxyphenyl group at the 7-position and these bonds result in the structural features of TEI-I01800. Moreover, the methyl group at the 6-position also causes a steric barrier to the *p*-ethoxyphenylamino group at the 7-position and determines the nonplanar conformation of TEI-I01800. As described above, TEI-I01800 can interact with the new binding pocket resulting from the conformational change from a β-sheet to an α-helix, allowing a favourable interaction between the *p*-ethoxyphenylamino group at the 7-position and Cys140 and Leu141. As the other inhibitors in published MK2–inhibitor structures do not contain a twisted functional group near Leu70, they are able to interact with β-form MK2 (Fig. 6). Therefore, the trigger of the conformational change is TEI-I01800 binding to avoid conflict with Leu70 of β-form MK2. Abbott Laboratories have recently reported a new MK2 (47–366, T222E mutant) and its complex with an inhibitor (Argiriadi *et al.*, 2009). The atomic coordinates of these structures have not yet been deposited in the PDB; however, the Gly-rich loop of the structure described in this study appears to form an α-helix. It is probable that this inhibitor may also regulate the secondary structure of the Gly-rich loop.

4. Conclusion

We determined the crystal structure of the MK2–TEI-I01800 complex. In the MK2–TEI-I01800 complex structure, we found that the Gly-rich loop adopted an α-helical confomation. TEI-I01800 has a nonplanar conformation, unlike other MK2 inhibitors. In order to avoid conflict with Leu70, TEI-I01800 causes a secondary-structural change of the Gly-rich loop from a β-sheet to an α-helix. The nonplanarity of TEI-I01800 allows it to make a stable inter-

action with the new binding pocket exposed by the α-form MK2. Previously, the presence of β-form MK2 had been considered to be a characteristic feature of an active kinase, as it had been found in all active MK2–small molecule complexes, but the present study shows that the α-helical Gly-rich loop of MK2 represents an active conformation that maintains the Lys93–Glu104 salt bridge. Moreover, the secondary structure of the Gly-rich loop is regulated by the structural features of the inhibitor.

TEI-I01800 shows good selectivity for MK2 against other kinases. Recently, the structure of the CDK2–TEI-I01800 complex was determined in our laboratory and its Gly-rich loop was found to adopt a β-sheet structure (A. Fujino, T. Kosugi & M. Takimoto-Kamimura, unpublished work). The difference in the inhibitory mechanism of TEI-I01800 is expected to make it useful as a new inhibitor with selectivity for MK2. The present study provides important information for the drug design of inhibitors accompanying the structural change of MK2.

We thank Professor I. Tanaka and Associate Professor M. Yao (Graduate School of Life Science, Hokkaido University) for their kind help in this research.

References

Anderson, D. R., Meyers, M. J., Kurumbail, R. G., Caspers, N., Poda, G. I., Long, S. A., Pierce, B. S., Mahoney, M. W., Mourey, R. J. & Parikh, M. D. (2009). *Bioorg. Med. Chem. Lett.* **19**, 4882–4884.

Anderson, D. R., Meyers, M. J., Vernier, W. F., Mahoney, M. W., Kurumbail, R. G., Caspers, N., Poda, G. I., Schindler, J. F., Reitz, D. B. & Mourey, R. J. (2007). *J. Med. Chem.* **50**, 2647–2654.

Argiriadi, M. A. *et al.* (2009). *BMC Struct. Biol.* **9**, 16.

Beyaert, R., Cuenda, A., Vanden Berghe, W., Plaisance, S., Lee, J. C., Haegeman, G., Cohen, P. & Fiers, W. (1996). *EMBO J.* **15**, 1914–1923.

Bricogne, G. (1974). *Acta Cryst.* A**30**, 395–405.

Collaborative Computational Project, Number 4 (1994). *Acta Cryst.* D**50**, 760–763.

Cowtan, K. (1994). *Jnt CCP4/ESF–EACBM Newsl. Protein Crystallogr.* **31**, 34–38.

Cuenda, A., Rouse, J., Doza, Y. N., Meier, R., Cohen, P., Gallagher, T. F., Young, P. R. & Lee, J. C. (1995). *FEBS Lett.* **364**, 229–233.

Goldberg, D. R. *et al.* (2008). *Bioorg. Med. Chem. Lett.* **18**, 938–941.

Gruenbaum, L. M., Schwartz, R., Woska, J. R. Jr, DeLeon, R. P., Peet, G. W., Warren, T. C., Capolino, A., Mara, L., Morelock, M. M., Shrutkowski, A., Jones, J. W. & Pargellis, C. A. (2009). *Biochem. Pharmacol.* **77**, 422–432.

Hillig, R. C., Eberspaecher, U., Monteclaro, F., Huber, M., Nguyen, D., Mengel, A., Muller-Tiemann, B. & Egner, U. (2007). *J. Mol. Biol.* **369**, 735–745.

Huse, M. & Kuriyan, J. (2002). *Cell*, **109**, 275–282.

Kotlyarov, A., Neininger, A., Schubert, C., Eckert, R., Birchmeier, C., Volk, H. D. & Gaestel, M. (1999). *Nature Cell Biol.* **1**, 94–97.

Kurumbail, R. G., Pawlitz, J. L., Stegeman, R. A., Stallings, W. C., Shieh, H.-S., Mourey, R. J., Bolten, S. L. & Brouadus, R. M. (2003). Patent WO/2003/076333.

Lee, J. C. *et al.* (1994). *Nature (London)*, **372**, 739–746.

Meng, W., Swenson, L. L., Fitzgibbon, M. J., Hayakawa, K., Ter Haar, E., Behrens, A. E., Fulghum, J. R. & Lippke, J. A. (2002). *J. Biol. Chem.* **277**, 37401–37405.

Murshudov, G. N., Vagin, A. A. & Dodson, E. J. (1997). *Acta Cryst.* D**53**, 240–255.

Otwinowski, Z. & Minor, W. (1997). *Methods Enzymol.* **276**, 307–326.

Pargellis, C., Tong, L., Churchill, L., Cirillo, P. F., Gilmore, T., Graham, A. G., Grob, P. M., Hickey, E. R., Moss, N., Pav, S. & Regan, J. (2002). *Nature Struct. Biol.* **9**, 268–272.

Schuller, D. J. (1996). *Acta Cryst.* D**52**, 425–434.

Underwood, K. W. *et al.* (2003). *Structure*, **11**, 627–636.

Vagin, A. & Teplyakov, A. (1997). *J. Appl. Cryst.* **30**, 1022–1025.

Wu, J. P. *et al.* (2007). *Bioorg. Med. Chem. Lett.* **17**, 4664–4669.

Xiong, Z., Gao, D. A., Cogan, D. A., Goldberg, D. R., Hao, M. H., Moss, N., Pack, E., Pargellis, C., Skow, D., Trieselmann, T., Werneburg, B. & White, A. (2008). *Bioorg. Med. Chem. Lett.* **18**, 1994–1999.

Yao, M., Zhou, Y. & Tanaka, I. (2006). *Acta Cryst.* D**62**, 189–196.

Zhou, Y., Yao, M. & Tanaka, I. (2006). *J. Appl. Cryst.* **39**, 57–63.